Macromolecules
ARTICLE

Macromolecules **2010**, *43*, 975–985 **975**
DOI: 10.1021/ma9020483

Effect of Hydroplasticization on Polymer Diffusion in Poly(butyl acrylate-*co*-methyl methacrylate) and Poly(2-ethylhexyl acrylate-*co*-*tert*-butyl methacrylate) Latex Films

Mohsen Soleimani,[†,‡] Jeffrey C. Haley,[‡] Willie Lau,[§] and Mitchell A. Winnik*[,†,‡]

[†]*Department of Chemical Engineering, University of Toronto, Toronto, Ontario, Canada, M5S 3E5,*
[‡]*Department of Chemistry, University of Toronto, Toronto, Ontario, Canada, M5S 3H6, and*
[§]*Dow Advanced Materials, The Dow Chemical Company, 727 Norristown Road, Spring House, Pennsylvania 19477*

Received September 14, 2009; Revised Manuscript Received November 23, 2009

ABSTRACT: We compare the influence of humidity on the polymer diffusion rate in films formed from two different polymer latex samples whose polymers have the same glass transition temperature ($T_g \approx 12$ °C) but different hydrophilicity: poly(butyl acrylate-*co*-methyl methacrylate), P(BA−MMA), and the more hydrophobic poly(2-ethylhexyl acrylate-*co*-*tert*-butyl methacrylate), P(EHA−tBMA). The diffusion process was monitored by fluorescence resonance energy transfer (FRET) at 25 °C and at 0, 23, 54, 85 and 98% relative humidities. The results show that the polymers diffused more rapidly in films aged at higher humidities, and thus were characterized by higher apparent diffusion coefficients (D_{app}). By performing a master curve analysis, we obtained humidity related shift factors (a_H). Not all the water taken up by these latex films contributes to enhance diffusion rates. Some of the water absorbed at high humidities is present in the form of water pools and microcavities (free water) and does not actively contribute to plasticization. We used FTIR spectra to obtain information about how water resides in the copolymer films. Although water is poorly miscible with most polymers, our results show that water molecules dispersed molecularly among the chains are highly efficient as a plasticizer and a promoter of polymer diffusion in latex films.

Introduction

Plasticizing polymers by incorporating small molecules as additives is a common strategy for modifying the mechanical properties of polymers.[1] At the molecular level, plasticizers affect intermolecular interactions and therefore chain relaxation dynamics by decreasing the internal friction coefficient among polymer chains. In this context, a variety of different organic compounds are intentionally introduced to polymer systems as plasticizers. For instance, in the coatings industry, volatile organic compounds (VOC) are often added to aqueous polymer latex formulations to decrease the modulus of polymer particles. In the presence of these volatile plasticizers, the particles become soft enough to deform and pack to yield transparent and void-free continuous films upon water evaporation. Over a longer time scale, as the VOCs escape to the atmosphere, the glass transition temperature (T_g) of the polymer film increases, and the film hardness increases.

Hydroplasticization, plasticization by moisture, often occurs unintentionally since water has limited but non-negligible solubility in many polymers. Despite its poor miscibility, moisture can lead to dramatic changes in the mechanical properties of a polymer. Hydroplasticization is more prominent for applications in which polymers are exposed to water rich media such as body fluids (e.g., tablet coatings, drug delivery systems, and implants)[2−5] or ambient moisture (e.g., polymer adhesives, automotive parts, latex paints, and coatings).[6−8] This problem is accentuated in water-based paints since they often contain salts and other hydrophilic additives.[8]

Moisture absorption into a polymer matrix is driven by osmotic pressure and proceeds until the activity of water absorbed into the polymer is equal to that in the vapor phase. For glassy polymers such as epoxy resins, the swelling stress may cause irreversible physical damage such as microcracking and crazing.[9] Moreover, the absorbed water can change the glass transition temperature of the polymer through the specific interaction of water molecules, disrupting interchain bonding networks[10] or by the composition dependence of the glass transition in miscible polymer-diluent systems.[11−13]

A large number of relationships between T_g and the phase composition of amorphous polymers have been developed. Aside from empirical equations, most of the theoretically driven relations such as the Fox, Gordon−Taylor or Kelly−Bueche equations are based on polymer free volume theory. For predicting the T_g of a moisture-softened polymer, the Couchman−Karasz equation is widely used. This expression modifies the Fox equation by taking into account changes in the specific heat capacity of water and that of the polymer ($\triangle C_p$) at T_g.[14] However, applying any predictive model requires a detailed understanding of how water resides in the polymer. The absorbed water may phase separate, as reported for many amorphous and crystalline polymers, such as epoxy resins,[19,23] cellulose esters,[15] poly(methyl methacrylate),[16] and poly(vinyl alcohol).[17,18]

The nature of absorbed water into epoxy resin has been thoroughly investigated.[12−23] Results based on quadrupole-echo NMR spectroscopy have indicated that water forms a single phase in epoxy polymers in which the water molecules present are more mobile than hydrogen-bonded water but less mobile compared to free water.[12,13] However, measurements employing other experimental techniques (such as dielectric measurements, FTIR, ATR−FTIR, UV−reflection, and positron annihilation lifetime spectroscopy) have been interpreted as indicating a dual nature of water in epoxy resin: a combination of molecularly bound water plus the presence of a more mobile water fraction localized in holes and cavities.[19−23]

*To whom correspondence should be addressed.

Published on Web 12/22/2009

Copolymers of acrylates and methacrylates are among the most widely used polymers in the coatings and adhesives industries. Hydroplasticization can occur for these materials as well.[24−26] Compared to epoxy resins, however, less attention has been paid to the structure of water absorbed in acrylate and methacrylate polymers. Clustering of water molecules in latex based films has been confirmed using forced Rayleigh scattering and NMR experiments.[27−29] A more detailed understanding of the hydroplasticization mechanism is required not only to avoid unintentional plasticization of acrylate coatings, but also to enable the use of water, a potential environmentally friendly plasticizer, to reduce VOC plasticizers in coating formulations.

As mentioned above, plasticizers are added to latex dispersions to reduce the modulus of the latex polymer and enhance the ease of particle deformation as particle dispersions dry to form films. Thus, the viscoelastic properties of the latex particles are the dominant resistive force against particle deformation in film formation. There are some suggestions in the literature that the viscoelastic properties of individual latex particles can differ significantly from those of the same polymer in the bulk state. These differences are thought to arise from the high surface area of the latex nanoparticles or from nanoconfinement effects associated with their small size. For example, Nawaz et al. studied crack patterns formed during drying of dispersions of cross-linked particles at different temperatures and drying times.[30] The drying time was increased by increasing humidity up to 80%. They reported that at longer drying times (i.e., higher humidities) less cracking occurred and crack spacing increased. Formation of cracks during the drying of latex dispersions has its origin in unrelaxed stresses within polymer particles. The authors obtained time temperature superposition (TTS) shift factors by analyzing the relation between the crack spacing and drying time. They reported that these shift factors are different from those obtained for the bulk polymer by rheology measurements. They concluded that the polymer in the particles has a different viscoelastic behavior compared to the same polymer in the bulk state and attributed this difference to the effect of nanoconfinement. Turshatov et al.[31] reported that the interparticle contact area is higher than what is expected from the minute extent of polymer diffusion that takes place during the drying of latex dispersions. They proposed the presence of a liquid-like low glass transition layer around the particles possibly due to nanoconfinement and hydroplasticization.

This study examines the influence of relative humidity on the diffusion rate in latex films of two copolymers, poly(butyl acrylate-*co*-methyl methacrylate) and poly(2-ethylhexyl acrylate-*co*-*tert*-butyl methacrylate), that differ in hydrophilicity but have the same glass transition ($T_g \approx 12$ °C). Polymer diffusion rates were measured by the fluorescence resonance energy transfer (FRET) technique using dye-labeled latex films. To investigate how moisture contributes to changes in free volume in the films, we also examine the influence of temperature on the polymer diffusion rates for films kept at low humidity. These experiments were combined with FTIR measurements to detect the presence of free water in the films at high humidities. In this way we present results that quantify the extent of hydroplasticization in the two different types of latex polymers and its influence on polymer diffusion rates.

Experimental Section

Materials. Potassium persulfate (KPS), sodium bicarbonate ($NaHCO_3$), 1-dodecanethiol (C_{12}−SH), and sodium dodecyl sulfate (SDS) were purchased from Aldrich and used as received. Methyl-β-cyclodextrin (Wacker Chemie) was used as a phase transport catalyst. Methyl methacrylate (MMA), tertiary butyl methacrylate (tBMA), butyl acrylate (BA), ethylhexyl acrylate (EHA) and methacrylic acid (MAA) were purified from hydroquinone inhibitors by passing through an inhibitor remover column (Aldrich). Phenanthrylmethyl methacrylate (PheMMA) was purchased from Toronto Research Chemicals Inc. and used without further purification. Dimethylamino-2-methacryloxy-5-methylbenzophenone (NBenMA) was provided by Rohm and Haas (synthesized as described previously by our group[38]) and was used as received. Water was purified by a Milli-Q ion exchange filtration system.

Table 1. Recipes for the Synthesis of Labeled and Nonlabeled Latex Dispersions

	amount of ingredient (g)		
ingredients (g)	seed latex	$P(EHA_{50}tBMA_{49})$ second stage	$P(BA_{50}MMA_{49})$ second stage
nonlabeled seed[a]		4.36	4.36
EHA (BA)		5	5
tBMA (MMA)	10	4.9	4.9
MAA		0.1	0.1
Phe−MMA[b]		0.1648	0.2425
or NBeN−MA[c]		0.0613	0.0851
C12-SH		0.025	0.025
SDS	0.5	0.2	0.2
$NaHCO_3$	0.1	0.055	0.055
KPS	0.1	0.6	0.6
methyl-β-cyclodextrin		0.075	0.075
water	90	6.35	6.35

[a] The same seed latex was used to synthesize all the latexes in this study. [b] Donor-labeled latexes were prepared by adding 1 mol % Phe-MMA. [c] Acceptor-labeled latexes were prepared by adding 0.3 mol % NBen-MA.

Latex Preparation and Characterization. All latexes in this study were synthesized by semicontinuous seeded emulsion polymerization under monomer-starved condition. An important feature of this reaction is that random copolymers, randomly labeled with fluorescence dyes can be synthesized regardless of the reactivity ratio of the species in the reaction.[32] Nonlabeled tBMA seed dispersion was synthesized by batch emulsion polymerization according to the recipe in Table 1. Water, SDS, and tBMA were mixed in a 250 mL three-neck flask equipped with a mechanical stirrer and a condenser. The mixture was stirred, purged thoroughly with nitrogen, and then immersed in an 80 °C thermostated oil bath. Buffered initiator solution (KPS, $NaHCO_3$ in 2 g water) was then injected into the flask, and the reaction was continued for 4 h. In the second stage, the seed particles were grown by seeded emulsion polymerization to a diameter of ca. 150 nm. A typical recipe for synthesizing nonlabeled poly(tBMA-*ran*-EHA-*ran*-MAA) is presented in Table 1. The recipe is designed to obtain latex at ca. 50% solids content.

An appropriate amount of the seed latex was mixed with methyl-β-cyclodextrin in a 100 mL three-neck flask, stirred, and purged thoroughly with nitrogen. The flask was then immersed in an 80 °C oil bath and the buffered initiator solution (KPS and $NaHCO_3$ in ca. 1 g water) was injected into the flask, followed by feed the monomer emulsion which was prepared by shaking the monomer mixture with an aqueous solution of SDS. The feeding rate was kept constant (0.08 mL/min) by a fluid metering pump (FMI-QG50). After feeding all the monomer emulsion, the reaction was continued for another 30 min. The flask was then allowed to cool down to room temperature. For labeled samples, the dye monomer was dissolved in the monomer mixture before making the monomer emulsion. Donor-labeled particles were prepared by adding 1 mol % (PheMMA); acceptor-labeled particles were prepared by

Table 2. Characterization of Latexes Used in This Study

sample	M_w	PDI	T_g (°C)[a]	d (nm)	polym[b]	solids content wt %
P($EHA_{50}tBMA_{49}$)	118 000	3.0	11.95	150	0.021	48.5
D−P($EHA_{50}tBMA_{49}$)	126 000	2.6	12.08	155	0.023	46.3
A−P($EHA_{50}tBMA_{49}$)	162 000	3.3	11.94	143	0.032	45.1
P($PBA_{50}MMA_{49}$)	185 000	2.4	12.14	146	0.048	48.2
D−P($PBA_{50}MMA_{49}$)	215 000	2.6	11.98	134	0.042	43.8
A−P($PBA_{50}MMA_{49}$)	227 000	3.2	12.22	150	0.036	48.4

[a] The glass transition is taken as the midpoint temperature of the deflection. [b] Particle size distribution as measured by the BI-90 particle sizer.

adding 0.3 mol % (NBen-MA) to the monomer mixture. After the synthesis, labeled latexes were kept in brown bottles and stored in the dark to prevent photodecomposition of the dyes.

Particle size and particle size distribution were measured by dynamic light scattering at 90° and at room temperature by a Brookhaven Instruments particle sizer (BI-90) equipped with a He−Ne laser. The solids content of latex samples was determined gravimetrically. The final compositions of the copolymers were determined by proton NMR in $CDCl_3$ using a Varian Mercury 300 MHz NMR spectrometer.

The glass transition temperature of each copolymer was measured with a TA Instruments Q100 differential scanning calorimeter (DSC). Samples were equilibrated at 150 °C and then scanned over a temperature range of −60 to 150 °C at a ramp of 10 °C/min for 2 complete cycles. The T_g values reported in Table 2 are taken as the midpoint temperature of the deflection in the second heating cycle.

Polymer molecular weights and polydispersity indices (PDI) were measured by gel permeation chromatography (GPC) using a Viscotek liquid chromatograph (TDA302) with tetrahydrofuran (THF) as the eluent (flow rate: 0.6 mL/min). The UV signal was collected with a UV detector (Viscotek 2501) at 300 nm for donor-labeled and at 350 nm for acceptor-labeled polymers. The molecular weights were determined based on a polystyrene calibration curve.

Gel content was measured by the centrifugation method developed in our laboratory.[33] Approximately 500 mg of each dried copolymer (W_1) was dissolved in 10 mL THF and agitated gently at room temperature overnight. Then, the solution was centrifuged at 20,000 rpm for 20 min (at 20 °C) with a Thermo Scientific Sorvall floor centrifuge. The precipitate (gel) was washed three more times with THF and dried overnight at 80 °C and weighed (W_2). The gel fraction is the ratio of W_2 to W_1.

Rheology Measurements. The linear viscoelastic response of copolymers was measured at several temperatures with a Rheometrics RAA instrument. Measurements were made in the oscillatory shear mode (from 0.01 to 100 s^{-1}) with parallel plate geometry (25 mm in diameter). Strain sweep tests were performed at each temperature to ensure that the data were collected in the linear viscoelastic regime. Samples were prepared from freeze-dried nonlabeled dispersion. Water can form hydrogen bonds with carboxylic acid groups in the copolymers. Therefore, it is hard to remove bonded water even at temperatures above T_g.[34] The absorbed water can form bubbles at high temperatures during the rheology experiments. To remove traces of water and other volatiles, the dried polymer was pressed at 120 °C in a Carver press. The polymer was placed in a 1 mm thick mold cavity and pressed between two clean Teflon sheets to obtain a clear bubble-free film. The Teflon plates were removed and the film was transferred between parallel plates at the time of the measurement.

FTIR Measurements. Fourier transform infrared (FTIR) spectra were obtained in the mid infrared range (4000−400 cm^{-1}) using a Perkin-Elmer Spectrum 1000. The spectra were measured with a resolution of 4 cm^{-1} and 32 scans to enhance the signal-to-noise ratio. Films (ca. 5 μm thick) of nonlabeled copolymers were prepared on glass slides (2 mm thick). The films were then equilibrated in chambers with fixed humidities. Before measuring the FTIR spectra, the films were covered with another glass slide to prevent water desorption during the measurement. To obtain the FTIR spectrum of dry polymer films, films were dried at 80 °C and under vacuum (ca. 10^{-4} Torr) overnight.

Glass has a cutoff value of 1850 cm^{-1} in the IR range and its IR absorption does not interfere with the OH stretching mode interval (4000−2600 cm^{-1}). To account for glass absorption in this range the background spectrum was measured with two glass slides mounted on the measurement window. For each film, the spectra were reproduced at least three times in different positions to ensure reproducibility. The spectra of water absorbed in the films were obtained by subtracting the background absorption of the polymer matrix.[35]

FRET Measurements. Latex films for energy transfer experiments were prepared from a mixture of donor- and acceptor-labeled particles. The appropriate weight of latex was determined in such a way that the final dried film contained 10% donor-labeled particles and 90% acceptor-labeled particles by weight. Aliquots of this dispersion were cast onto quartz plates (20 × 8 mm) and dried uncovered in a cold room (10 °C). Under this condition, we were able to obtain clear, transparent, and crack-free films without noticeable mixing of donor- and acceptor-labeled chains. To check the final value of energy transfer, we brought the D- and A-labeled chains to a fully mixed state by adding several drops of THF to the film. The THF was evaporated slowly at room temperature and this procedure was repeated three times. The remaining traces of THF were removed by annealing at 70 °C overnight. From fluorescence decay measurements on these films, we obtained the maximum experimentally achievable fraction of mixing.

For annealing film samples at different temperatures, the films on quartz plates were placed on a high mass aluminum plate (ca. 3 cm thick) preheated to the desired annealing temperature in a forced-air convection oven (Fisher scientific, Model 496). To stop diffusion before each decay measurement, films were placed for 1 min on another thick aluminum plate kept at 3 °C. Fluorescence decays were measured by the time correlated single photon counting technique. A 296 nm pulsed diode (NanoLED, IBH) was used as excitation source and the fluorescence emission was collected at 350 nm using a monochromator (IBH) and was detected by an air-cooled photon detection module (TBX-04, IBH). A 335 nm cutoff filter was mounted on the emission monochromator window to reduce the intensity of scattered light at the detector. Data were collected until 5000 counts were accumulated in the maximum channel. The instrument response function was obtained by using a mimic standard, which was a degassed solution of *p*-terphenyl with a 0.96 ns

lifetime.[36] This decay reflects the width of the excitation source and the instrument response time associated with counting photons.

To investigate the effects of humidity on diffusion rate, we prepared chambers with fixed humidity using saturated salt solutions. Four hermetic chambers were prepared with 23%, 54%, 85%, and 98% relative humidities (RH) at 25 °C using saturated solutions of potassium acetate, magnesium nitrate, potassium chloride, and potassium sulfate, respectively.[37] The humidity in each chamber was checked by a thermohygrometer (T2041, Aldrich). We used silica gel as a desiccant to obtain near-zero humidity condition. The humidity in this chamber was checked throughout the experiment by a humidity sensor (HM1520F, Humirel) and was $0 \pm 2\%$. The chambers were relatively small (~500 mL), so they could rapidly reach the equilibrium humidity compared to the time scale of the experiments (days).

All chambers were kept in a free convection oven (Yamata DX300) at 25 °C during the experiment. The films were removed from the chambers periodically, and the fluorescence decays were measured as described above. Each measurement took at most 2 min, much shorter than the time frame of the experiment. Therefore, we do not expect exposure to ambient conditions to affect our results significantly.

The equilibrium water content of the copolymers at different humidities was measured gravimetrically with a Mettler Toledo model MX5 microbalance. Nonlabeled copolymer films (ca. 500 mg) were prepared on Teflon sheets and dried in vacuum oven at 80 °C for 24 h. These films were equilibrated in the hermetic chambers and weighed afterward. To test the possibility of capillary condensation, we remeasured the equilibrium water content for films cast and dried at 10 °C, equilibrated at each humidity and at 25 °C (the same condition for the films prepared for FRET measurements). Then the films were dried at 80 °C and under vacuum overnight. We did not observe a significant difference between the results of these two methods and thus ruled out occurrence of capillary condensation for films dried at 10 °C.

Data and Data Analysis

FRET is a nonradiative process by which energy is transferred between two chromophores, a donor dye and an acceptor dye, through dipole−dipole interactions. The rate of energy transfer (w) is a strong function of the distance between the donor and the acceptor (R)

$$w(r) = \frac{3\kappa^2}{2\tau_D}\left(\frac{R_0}{R}\right)^6 \tag{1}$$

where κ^2 is related to the average orientation of donor- and acceptor-dipoles and has the value 0.476 for a random orientation of immobile chromophores in three-dimensional space, a typical situation for dyes embedded in polymer matrices.[38,39] R_0 is the critical Förster distance for energy transfer at which radiative and nonradiative processes have equal rates. For the Phe/NBen pair R_0 takes a value of 2.51 ± 0.04 nm.[40] τ_D is the donor lifetime in the absence of acceptors. The donor (Phe) decays exponentially with $\tau_D = 44.4$ ns for both copolymers studied here.

Films containing both donors and acceptors are characterized by nonexponential donor fluorescence decays whose shape depends upon the details of the donor and acceptor distribution. For a uniform distribution of donors and acceptors, the donor fluorescence intensity decay following instantaneous (delta-pulse) excitation $I_D(t)$ is given by the Förster equation:[41]

$$I_D(t') = A \exp\left[\frac{-t'}{\tau_D} - P\left(\frac{t'}{\tau_D}\right)^{1/2}\right] \tag{2a}$$

$$P = \frac{4}{3}\pi^{3/2} N_A \left\langle \frac{3}{2}\kappa^2 \right\rangle^{1/2} {R_0}^3 C_A \tag{2b}$$

in which C_A is the acceptor concentration and N_A is the Avogadro number.

In a latex film cast from a mixture of donor- and acceptor-labeled particles, the distribution of chromophores changes as diffusion takes place. For films prepared from a 1:9 ratio of donor-to-acceptor labeled particles, we modeled the diffusion process by assuming that each donor-labeled particle is surrounded by an acceptor-labeled-shell. The thickness of the shell in this core−shell geometry was adjusted in such a way that the core volume fraction was equal to the volume fraction of donor-labeled particles used to prepare the film. The net mass flux across the outer boundary of the shell was set to zero throughout the calculations. For this geometry, the normalized donor- and acceptor-concentration as a function of distance from the particle center (r) and extent of diffusion (x, $x^2 = Dt$) can be derived assuming a Fickian diffusion mechanism (see eq S1 in the Supporting Information).[42]

We used these normalized concentration profiles (C_A and C_D) as probability density functions to generate ensembles of donors and acceptors by a Monte Carlo sampling technique. We increased the number of donor dyes until the results (the calculated decays) were independent of the actual number of donors. Therefore, the number of donors (ca. 50 000) was large enough to guarantee the statistical stability of the model. Donors and acceptors may be placed within a distance a of the particle center. To ensure that energy transfer from the donors located near the outer boundary is properly taken into account, an additional layer ($5R_0$ in thickness) containing acceptors with a concentration of $C_A(a)$ was added to the outer shell. On the basis of eq 1, the rate of energy transfer can be shown to be negligible for a donor and an acceptor separated by more than $5R_0$.

The simulation locates every donor and acceptor placed in the system and calculates the quantum efficiency of energy transfer (Φ_{ET}) and the fluorescence decay of the donor after delta-pulse excitation ($I_D(t')$).[43,44] More details about the calculation procedure are provided in the Supporting Information.

We generated a series of donor decay profiles representing increasing extents of diffusion (x). These trial $I_{D/A}(t')$ profiles were then convoluted with the instrument response function corresponding to an experiment and then compared through a fitting analysis to the experimentally measured decay profile. For the best fit, values of the χ^2 parameter were between 0.95 and 1.2, and the plots of weighted residuals and the autocorrelation function of weighted residuals were randomly distributed around zero. The diffusion coefficient was calculated by dividing x^2 by the annealing time (t). The simulation analysis assumes that a mean value of D_{app} describes the Fickian diffusion that has taken place over all times up to t.

The fractional growth in the quantum efficiency of energy transfer (f_m) was calculated as:

$$f_m(t) = \frac{\Phi_{ET}(t) - \Phi_{ET}(0)}{\Phi_{ET}(\infty) - \Phi_{ET}(0)} \tag{3}$$

Here $\Phi_{ET}(0)$ is the initial value of the energy transfer quantum efficiency for donors and acceptors distributed on opposite sides

of the core−shell boundary at the start of the experiment. $\Phi_{ET}(\infty)$ is the final value of the energy transfer quantum efficiency following complete mixing of donors and acceptors. These values were calculated from the simulations for $x = 0$ and $x = 1000$, respectively. One anticipates that the system will become fully mixed at high extents of diffusion, with Φ_{ET} reaching a plateau. This behavior was followed in the simulations.

Results and Discussion

Preparation and Characterization of Latex Samples. The latex particles examined here were synthesized by seeded emulsion polymerization.[45,46] The use of a common seed latex for all syntheses facilitates obtaining latex particle samples of similar size and with polymers of similar molecular weight and molecular weight distribution.[40] The seed particles we employed were 50 nm in diameter. Therefore, it contributes only a small fraction (ca. 4%) of unlabeled polymer to the final particle.

The more hydrophobic copolymer consists of 50 wt % EHA, 49 wt % tBMA, and 1 wt % MAA. The more hydrophilic system is a copolymer of 50 wt % BA, 49 wt % MMA, and 1 wt % MAA. Such small amounts of methacrylic acid are commonly used in the synthesis of commercial latex for coatings to enhance the colloidal stability of the latex. In the case of the more hydrophobic latex, methacrylic acid helped ensure effective and complete polymerization in the second stage reaction. When MAA was eliminated from the hydrophobic copolymer recipe, i.e., for P($EHA_{50}tBMA_{50}$), a shoulder appeared at high molecular weight in the GPC trace. We believe the high molecular weight chains are formed due to a higher rate of bimolecular termination caused by the poor solubility of both EHA and tBMA in water during the polymerization. We speculate that incorporation of small amounts of MAA helps with keeping the radicals active in the growing latex particles. We do not include "MAA" in our notation for the samples. Thus, the copolymers are referred to as P($EHA_{50}tBMA_{49}$) and P($BA_{50}MMA_{49}$) according to their composition.

Our main objective in designing the synthesis of these latexes was to obtain samples with a similar glass transition temperature (with a target of $T_g = 12$ °C), high molecular weight and low gel content. We could suppress gel formation effectively by adding 0.25 wt % C_{12}−SH without excessively decreasing the molecular weight. The methyl-β-cyclodextrin in the recipe helps to transport of C_{12}−SH during the reaction. The gel fraction of copolymers was below 4 wt %. The samples obtained had T_g values very close to 12 °C, and these values were not affected by labeling the polymer with fluorescence dyes (Table 2).

In all GPC traces, the UV signal (which monitors the dyes) followed the shape of the refractive index (RI) signal (which monitors the polymer). This result indicates that the polymer chains are randomly labeled with fluorescence dyes. The characterization data for all latex samples are listed in Table 2. The molecular weight and PDI of the labeled samples are close to those of the nonlabeled samples. The final composition of the copolymers, as determined by proton NMR, was close to the composition of the initial monomer mixture. All dispersions have particle diameters narrowly distributed around 150 nm.

Energy Transfer Studies of Polymer Diffusion. Energy transfer experiments were carried out on mixtures containing 10% donor-labeled particles and 90% acceptor-labeled particles. This acceptor-rich mixture was chosen to facilitate simulations of experiments in which a donor-labeled sphere is treated as though it is surrounded by acceptor-labeled polymer. As donor- and acceptor-labeled chains diffuse together, more donors come into proximity with acceptors. In time-resolved experiments, the donor decay ($I_D(t')$) becomes more rapid as the fraction of mixing increases.

Table 3. The Initial and Final Energy Transfer Efficiency $\Phi_{ET}(0)$

	P($EHA_{50}tBMA_{49}$)		P($BA_{50}MMA_{49}$)	
	$\Phi_{ET}(0)$	$\Phi_{ET}(\infty)$	$\Phi_{ET}(0)$	$\Phi_{ET}(\infty)$
simulated[a,b]	0.024	0.52	0.038	0.65
experimental	0.046	0.50	0.072	0.63

[a] The simulated values were obtained for $x^2 = 0$ ($\Phi_{ET}(0)$) and $x^2 = 1000\Phi_{ET}(\infty)$. [b] x represents the diffusion depth ($x^2 = Dt$) of the donor- or acceptor-labeled chains.

To prepare samples for FRET measurements, aliquots of the D/A mixed latex were cast on small quartz plates and dried at 10 °C. Drying samples at low temperature minimizes any polymer diffusion that might take place as the water evaporates. The initial values of energy transfer efficiency (Φ_{ET}) were determined for each mixture. Final (limiting) values of Φ_{ET} were obtained by taking representative film samples of each composition, adding drops of THF to dissolve the polymer and promote mixing and then letting the THF evaporate. These initial and final values of Φ_{ET} were then compared to values obtained in our Monte Carlo simulations (Table 3).

In the Monte Carlo simulations, $x = 0$ corresponds to the situation where no polymer diffusion has taken place ($x^2 = Dt$, $t = 0$). At $x = 0$, the simulated value of Φ_{ET} is not zero because a small extent of energy transfer takes place between donors and acceptors on opposite sides of the boundary between donor- and acceptor-labeled particles. Previous experiments and simulations in our group have indicated that the assumption of a sharp interface between 120 nm labeled particles leads to a value of 0.05−0.07 for $\Phi_{ET}(0)$.[47] For the 150 nm diameter particles employed here, the Monte Carlo calculations predict slightly smaller values of $\Phi_{ET}(0)$ (see Table 3), consistent with a reduced interfacial area compared to 120 nm diameter particles.

The measured values are slightly larger than the predicted values. These small differences can be explained by possible surface roughness in latex particles or a small extent of oligomer diffusion during the drying process. Simulated values of Φ_{ET} corresponding to the fully mixed state are in very good accord with measured $\Phi_{ET}(\infty)$ values. For consistency in calculating fractions of mixing f_m (eq 3), we will use values for $\Phi_{ET}(0)$ and $\Phi_{ET}(\infty)$ obtained from the Monte Carlo simulations.

Polymer Diffusion at Different Temperatures. Although the focus of this paper is on humidity effects on polymer diffusion, interpreting those data will require information that is only available from variable temperature experiments. Thus, in this section, we describe experiments that examine how temperature affects the rate of polymer diffusion for both P($EHA_{50}tBMA_{49}$) and P($BA_{50}MMA_{49}$) and interpret these data in terms of free volume changes in the polymer films. Information about free volume changes was obtained from dynamic mechanical measurements (G', G'') over a somewhat broader range of temperatures. We will keep the detail here brief and will provide more information in the Supporting Information.

Donor fluorescence decay profiles were measured as a function of annealing time at each of four temperatures (40, 50, 60, and 70 °C) for both polymer samples. For each decay, we found the best simulated $I_{D/A}(t')$ that can represent the measured decay. From the simulated decay, we obtained in turn the extent of diffusion (x) and the apparent diffusion

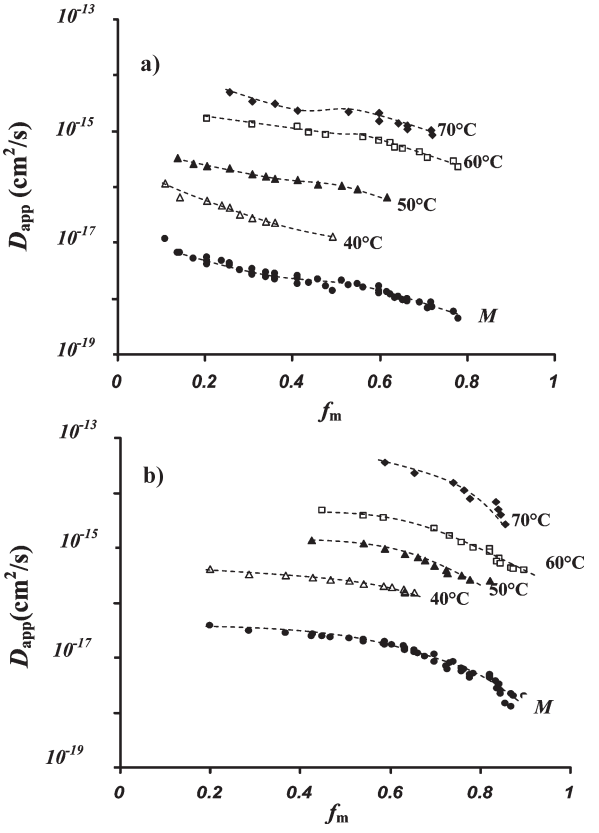

Figure 1. Plots of the apparent diffusion coefficient D_{app} vs fraction of mixing f_m for a) P($BA_{50}MMA_{49}$) and b) P($EHA_{50}tBMA_{49}$) at 40, 50, 60, and 70 °C. The master curves are shifted one unit down for clarity. For P($BA_{50}MMA_{49}$), E_a = 38.5 kcal/mol and for P($EHA_{50}tBMA_{49}$), E_a = 35.7 kcal/mol were used as shift factors.

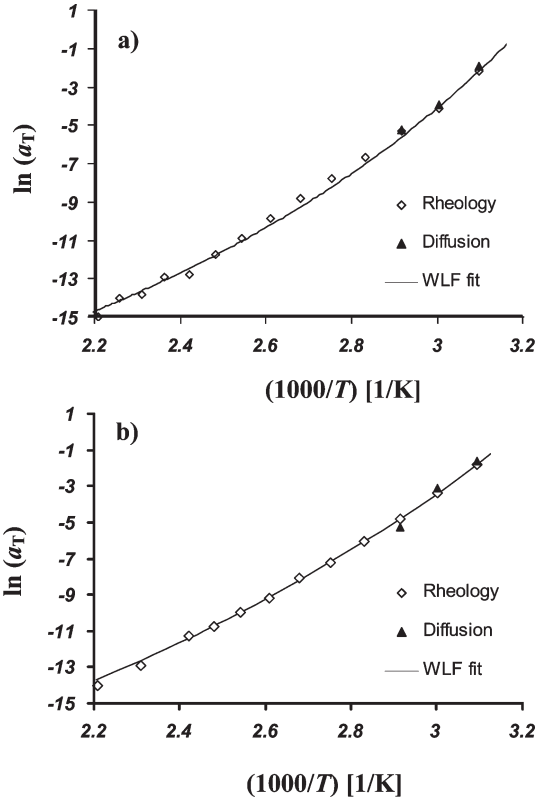

Figure 2. Plots of the ln(a_T) against the inverse of the absolute temperatures for a) P($BA_{50}MMA_{49}$) and b) P($EHA_{50}tBMA_{49}$).

coefficient (D_{app}). These values are presented in Figure 1. At each annealing time, D_{app} is a weighted average of the diffusion coefficient of species that have diffused up to that time.[40] Values of Φ_{ET} were calculated via eq S3b (Supporting Information), and then mixing fraction f_m was calculated with eq 3 using simulated values for $\Phi_{ET}(0)$ and $\Phi_{ET}(\infty)$ (Table 3). Plots of the evolution of Φ_{ET} and f_m over time are presented in Figures S1 and S2 in the Supporting Information.

The curves in Figure 1 show that for experiments carried out at higher temperatures, meaningful data could be obtained beginning only from higher values of f_m. In these experiments, it becomes increasingly challenging to track diffusion at high temperatures. One important feature associated with finding a common Master Curve for these data is that it is possible to extrapolate back to early extents of mixing for these high temperatures. This is a typical feature of time−temperature superposition common to many different types of polymer dynamics experiments.

Polymer dynamics above the glass transition temperature is mainly governed by the chain length and the monomer friction coefficient (ζ_0). ζ_0 represents the friction force per monomer unit of a chain as it moves with unit velocity through a medium consisting of same chains.[48] At low molecular weights, ζ_0 increases with decreasing chain length due to the additional free volume associated with chain ends. The molecular weights of the samples in this study are high enough to neglect the effect of molecular weight on ζ_0. This might not be the case at the very early stages of mixing (oligomer diffusion at very low f_m), but it certainly holds during the rest of the mixing process. Therefore, ζ_0 was treated as a constant at each temperature. A consequence of this assumption is that the apparent activation energy for overcoming diffusion barriers in bulk (E_a) should be constant over all mixing fractions. Indeed, plots of ln(D_{app}) vs 1/T at two different f_m values were linear (see Figure S3 in Supporting Information), and the activation energies obtained could be used as shift factors to shift the diffusion data in Figure 1 to a common master curve for each polymer.

We performed rheology measurements to confirm shift factors obtained from FRET. The master curves built by shifting storage (G') and loss modulus (G'') data for nonlabeled copolymers are presented in the Supporting Information. Figure 2 shows that good correlation exists between shift factors obtained by two different experiments. We fit the Williams−Landel−Ferry (WLF) equation to the shift factors and obtained WLF constants for each copolymer.

Our goal here was first, to ensure that the diffusion behavior of our systems complies with the WLF equation, a free volume based model and second, to show agreement between diffusion experiments (using FRET) and rheological measurements. From the WLF fit to the data (Figure 2), we obtained the WLF parameters for both copolymers at a reference temperature of 40 °C. For P($BA_{50}MMA_{49}$), C_1 = 21.2 and C_2 = 107.8; for P($EHA_{50}tBMA_{49}$), C_1 = 27.6 and C_2 = 141.9.

Effect of Humidity on Polymer Diffusion: Hydroplasticization. High humidity slows down the drying, so chains in the dried edge of the film have more time to diffuse.[49] To separate the effects of humidity on the drying rate from its effects on long-term diffusion, we dried all the films at ca. 0% RH and 10 °C. The films were then transferred to hermetic chambers with fixed relative humidity for the rest of experiment. The films were 30−40 μm thick and equilibrated rapidly with RH. Following this procedure, the initial f_m values for all films were nearly the same. Therefore, the

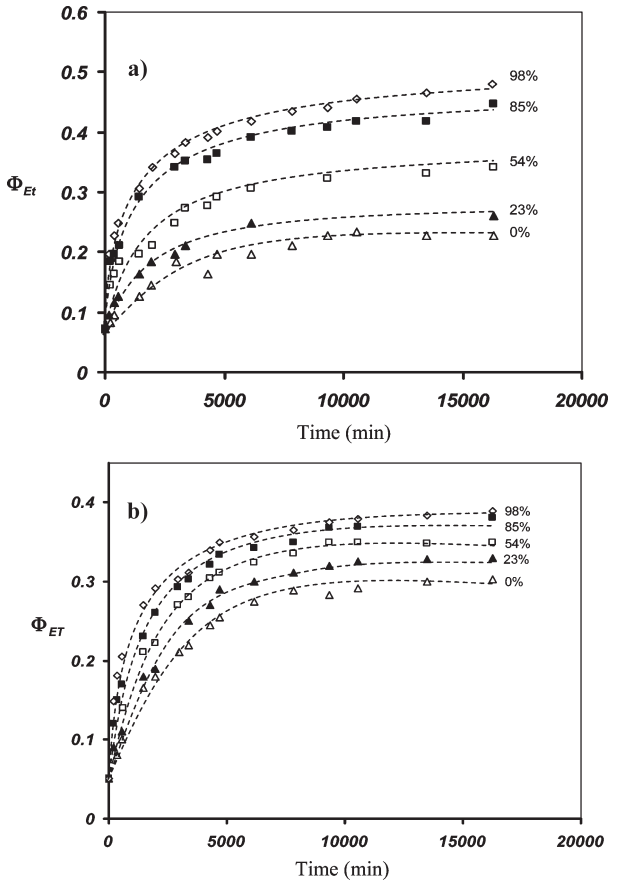

Figure 3. Plots of the energy transfer efficiency Φ_{ET} vs time for (a) $P(BA_{50}MMA_{49})$ and (b) $P(EHA_{50}tBMA_{49})$ at 0, 23, 54, 85, and 98% RH and 25 °C.

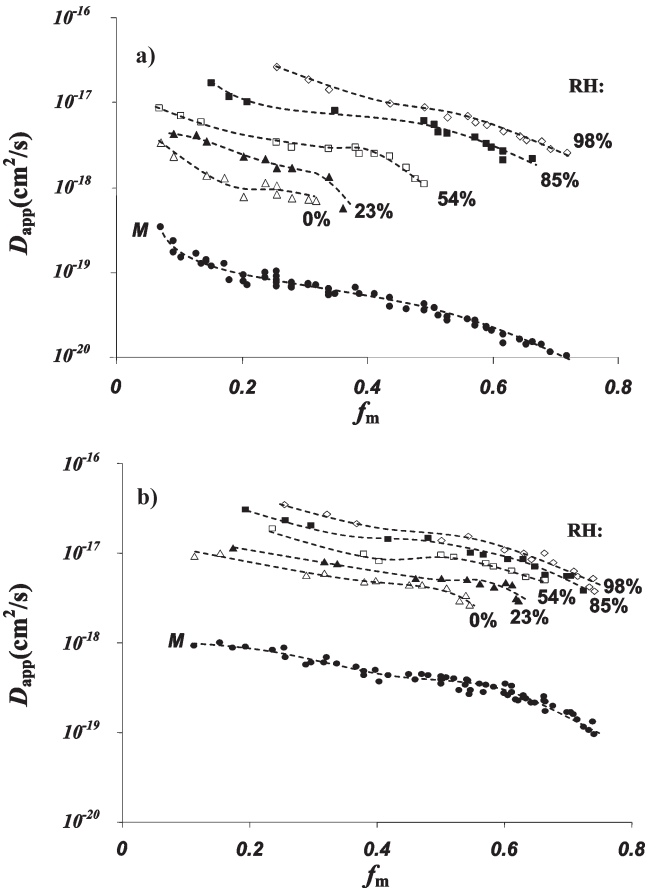

Figure 4. Plots of the apparent diffusion coefficient D_{app} vs aging time for (a) $P(BA_{50}MMA_{49})$ and (b) $P(EHA_{50}tBMA_{49})$ at 0, 23, 54, 85, and 98% RH and 25 °C. The master curves are shifted one unit down for clarity.

observed differences in the evolution of f_m values are solely due to hydroplasticization and not due to different initial values of f_m.

Figure 3 shows plots of Φ_{ET} values determined by periodically removing samples from the chambers, rapidly measuring their decay profile ($I_{D/A}(t)$), and then returning them to the constant humidity chambers again. In general, Φ_{ET} values increase more rapidly at higher humidities. The evolution of Φ_{ET} in $P(BA_{50}MMA_{49})$ strongly depends on humidity, whereas it shows less sensitivity to humidity in $P(EHA_{50}tBMA_{49})$. Similar trends were revealed when f_m values (calculated by eq 3, using simulated values of $\Phi_{ET}(0)$ and $\Phi_{ET}(\infty)$ from Table 3) were plotted against aging time.

In Figure 4, D_{app} values are plotted versus f_m for $P(BA_{50}MMA_{49})$ and $P(EHA_{50}tBMA_{49})$. Here, and also in Figure 1, D_{app} values drop by nearly an order of magnitude as the fraction of mixing increases. We attribute this to the contribution of slowly diffusing species such as high molecular weight polymer or possibly branched chains that takes place at higher mixing fractions. As f_m approaches unity, energy transfer measurements lose their sensitivity to diffusion.

The diffusion coefficient values for $P(BA_{50}MMA_{49})$ are lower than those for $P(EHA_{50}tBMA_{49})$ by nearly an order of magnitude. This is likely a reflection of the difference in molecular weight of the samples. The acceptor-labeled $P(BA_{50}MMA_{49})$ had a M_w of 227 000 whereas M_w = 162 000 for acceptor-labeled $P(EHA_{50}tBMA_{49})$.

Analogous to how we studied the effect of temperature on diffusion, we built master curves by using vertical shift factors (a_H) that overlay the curves recorded at different relative humidity values (RHs) on the one recorded at zero humidity. For both copolymers, the D_{app} values associated with the humidity master curve (at 0% RH and 25 °C) are at least 2 orders of magnitude lower than those shown in Figure 1 with a reference temperature of 40 °C (and 0% RH). The detailed shape of the master curve is primarily determined by the details of molecular weight distribution. Therefore, for each copolymer, the shape of the master curves is similar regardless of the reference temperature.

Table 4. Vertical Shift Factors and Equilibrium Water Content at Different Humidities

	$P(BA_{50}MMA_{49})$		$P(EHA_{50}tBMA_{49})$	
RH, %	water, wt %	a_H	water, wt %	a_H
0		1		1
23	0.30	1.9	0.20	1.45
54	0.90	5.2	0.60	2.75
85	2.40	16.4	1.80	3.3
98	9.00	30.0	5.14	4.1

The shift factors are a measure of the extent of hydroplasticization. The results show that water absorbed by the film accelerates diffusion by a factor of 30 in $P(BA_{50}MMA_{49})$ whereas this factor is only 4 for $P(EHA_{50}tBMA_{49})$. To make these data more comprehensible, we measured the equilibrium water content gravimetrically. Table 4 shows the equilibrium water content along with the a_H values. At 85% relative humidity, $P(BA_{50}MMA_{49})$ picks up 2.4 wt % water whereas $P(EHA_{50}tBMA_{49})$ peaks up 1.8 wt % water.

We observed visually that both films became turbid at 98% RH. This indicates the presence of phase separated regions of sufficient size to scatter visible light.

To analyze these data quantitatively, we assume that moisture plasticizes the polymer by decreasing the magnitude of the monomer friction coefficient (ζ_0). For each sample, the polymer diffusion rate depends upon the difference ($T - T_g$). Since the measurements were performed at a constant temperature, the influence of moisture is to decrease T_g.

In the previous section, where the free volume increased as a consequence of increasing temperature, we could use TTS to obtain temperature shift factors (a_T). The WLF equation could fit the a_T values obtained at different $\triangle T$. Similarly, it is possible to use a_H values and obtain $\triangle T$ from the WLF equation. Unlike measurements at different temperatures, in the humidity experiments, the experimental temperature is constant and $\triangle T$ originates from a relative decrease in samples T_g due to hydroplasticization.

$$C_{2,T} = C_{2,T_0} - (T_0 - T) \tag{4}$$

$$C_{1,T} = \frac{C_{1,T_0} C_{2,T_0}}{C_{2,T}}$$

By shifting the WLF parameter to the glass transition temperature[48] (eq 4) we estimated the depression in the glass transition of P($BA_{50}MMA_{49}$) and P($EHA_{50}tBMA_{49}$) at 98% RH to be 8.5 and 4.5 °C, respectively. These values are comparable to what Sperry et al. reported for the difference between wet and dry minimum film formation temperature.[24] Nawaz et al. reported a 20 °C drop in the glass transition for 50 nm PBMA particles,[30] which is indeed higher than what can be explained by hydroplasticization alone.

We want to emphasize that this analysis is independent of the state of water in the film. However, fundamentally the WLF parameters for the plasticized and the unplasticized system may not be the same. In other words, a plasticizer might specifically affect a given relaxation process besides decreasing ζ_0. It has been shown that moisture does not accelerate or retard a given relaxation process in polymers.[50] Having measured the WLF constants, we preferred to extend these parameters to the plasticized state since predictive models for glass transition of hydroplasticized samples do not provide an accurate estimate.[51]

If water acts as a traditional plasticizer and uniformly increases the free volume throughout the sample, it should be possible to fit the Fujita−Doolittle equation to the data presented in Table 4. Fujita proposed a linear increase in the polymer free volume with the volume fraction of added plasticizer (φ) (eq 5).[52] Here, $\beta(T)$ is the difference between the fractional free volume of the polymer and that of the plasticizer at temperature T, and $f(0, T)$ is the fractional free volume of pure polymer; $\beta(T)$ is the factor by which the free volume increases, and its magnitude is a measure of the plasticizer efficiency.

$$f(\varphi_1, T) = f(0, T) + \beta(T) \times \varphi_w \tag{5}$$

Fujita showed that combining eq 5 with the Doolittle equation makes it possible to predict the viscosity and the diffusion coefficient of a plasticized polymer (eq 6). We attempted to fit the data in Table 4 to the Fujita-Doolittle model. We assumed equal density for water and polymer so that we could use wt % instead of vol %.

Table 5. Spectroscopic Parameters of Water Absorbed to P-($BA_{50}MMA_{49}$) at Different Water Activities in the Film (Relative Humidity)

a_w	position ± 2 (cm^{-1})	intensity	fwhm(cm^{-1})	relative area(%)
	3280	0.112	308	46.5
0.98	3445	0.148	185	32.1
	3561	0.124	126	17.0
	3636	0.061	66	4.4
	3280	0.040	320	38.7
0.85	3445	0.053	179	28.7
	3561	0.066	127	25.3
	3636	0.037	65	7.3
	3280			
0.54	3445	0.020	133	37.5
	3561	0.030	114	49.0
	3636	0.017	55	13.5
	3280			
0.23	3445	0.007	108	20
	3561	0.019	110	57.5
	3636	0.014	58	22.5

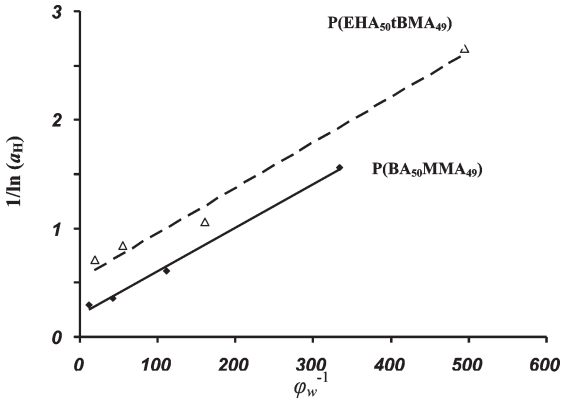

Figure 5. Plots of $1/\ln(a_H)$ vs φ_w^{-1} based on the data in Table 4 For P($EHA_{50}tBMA_{49}$) the intercept and slope of the line are 0.530 and 0.004 respectively ($R^2 = 0.97$). For P($BA_{50}MMA_{49}$) the intercept and slope of the line are 0.205 and 0.004 respectively ($R^2 = 0.99$).

$$\left(\frac{1}{\ln(D(T,\varphi_w)/D(T,0))}\right) = \left(\frac{1}{\ln(a_H)}\right) = f(0,T) + \frac{f(0,T)^2}{\beta(T)}\left(\frac{1}{\varphi_w}\right) \tag{6}$$

Figure 5 illustrates these Fujita plots. As predicted by eq 6, we obtained a linear relation between $1/\ln(a_H)$ and $1/\varphi_w$. However, the parameters obtained from these lines do not conform to the theoretical expectations. These plots lead to β values of ca. 10.5 for P($EHA_{50}tBMA_{49}$) and 67 for P-($BA_{50}MMA_{49}$), respectively. These values are much higher than reported values for other plasticizers; but more significantly, are contradictory to the definition that β cannot be greater than unity. In addition, the magnitude of the intercept does not match the value we[53,54] and others[52] obtained previously. The intercept of the Fujita fit is proportional to the free volume of the pure polymer ($f(0,T)$) at the experimental temperature. Following the WLF approach, one can show that $f(0,T) = 1/C_1$, where C_1 is the first WLF parameter at the experimental temperature.

At 25 °C, the values of $1/C_1$ are 0.032 and 0.041 for P($EHA_{50}tBMA_{49}$) and P($BA_{50}MMA_{49}$) respectively. If we fix the intercept at these values and attempt to fit the data to the Fujita equation, the correlation coefficient (R^2) decreases

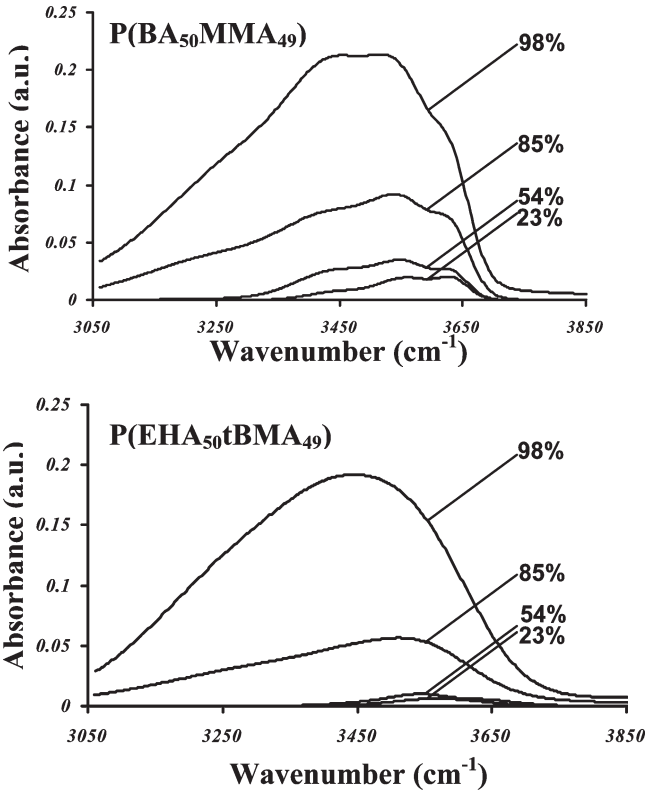

Figure 6. FTIR spectra (in the OH stretching region) of water absorbed into the copolymer films at different relative humidities.

mildly for the hydrophilic $P(BA_{50}MMA_{49})$ but significantly for hydrophobic $P(EHA_{50}tBMA_{49})$ as shown in Figure S5 in the Supporting Information. In addition, the deviation of experimental data from the Fujita prediction is more prominent for films aged at higher humidities.

FTIR Analysis of Water Content in the Films. In assessing the efficiency of water insoluble plasticizers such as Texanol (2,2,4-trimethyl-1,3-pentanediol monoisobutyrate), partitioning of the plasticizer plays a key role. The partition coefficient determines how plasticizer is partitioned between the water and the polymer phase. Evidently, the fraction of plasticizer in the water phase does not contribute to the plasticization process and should not be taken into account for calculating the β parameter. In the experiment described above, only water molecules that are molecularly dispersed among the polymer chains can serve as plasticizer and increase the free volume. Water that resides in a phase-separated state will not contribute in this way.

Phase separation of absorbed water in polymers has been reported for many polymers and resins.[17−19,23] The important question that arises is at which point water starts to phase separate from the film. Figure 6 shows FTIR spectra in the ν_{OH} stretching region for both copolymers. The major feature of the spectra is that the intensity of the broad unresolved ν_{OH} band (in the region 3050−3700 cm^{-1}) increases at higher humidities.

The unresolved ν_{OH} interval corresponds to the different states of water that reside in the film i.e hydrogen bonded water, water monomers, dimers and free water.[19,16] The reason for the appearance of several bands is that the time scale of vibration is much shorter than the time scale of hydrogen bond formation.[16] To resolve the ν_{OH} multicomponent band we used a curve-fitting algorithm based on the Levenberg−Marquardt minimization method. In all cases, we used mixed Gaussian−Lorentzian peaks.[55] For each copolymer, the baseline, band shape and the number of components were fixed and the minimization algorithm was allowed to find the height, position, and full width at half-maximum (fwhm) of each peak.

Table 6. Spectroscopic Parameters of Water Absorbed to P-($EHA_{50}tBMA_{49}$) at Different Water Activities in the Film (Relative Humidity)[a]

a_w	position ± 2 (cm^{-1})	intensity	fwhm(cm^{-1})	relative area (%)
	3336	0.142	365	66.2
0.98	3515	0.104	243	33.8
	3336	0.030	438	58.8
0.85	3515	0.040	237	41.2
	3336			
0.54	3515	0.009	201	100

[a] At a_w = 0.23 the analysis was not possible due to very low water content.

To reduce the number of fitting parameters, we used the minimum number of bands that would afford a good fit to the experimental spectra. For $P(BA_{50}MMA_{49})$, at least four bands are needed to resolve the peak with good fitting quality (judged by minimizing χ^2). Figure S7 represents an example of resolved bands for the $P(BA_{50}MMA_{49})$ film at 98% relative humidity. In case of $P(EHA_{50}tBMA_{49})$, using two bands results in accurate representation of the FTIR spectra. Figure S8 shows the curve-fitting analysis results for $P(EHA_{50}tBMA_{49})$ at 98% relative humidity. $P(EHA_{50}tBMA_{49})$ absorbed ca. 0.2 wt % water at 23% RH. The isolated FTIR spectrum of this sample was noisy with weak intensity. Therefore, we could not resolve the peaks meaningfully by the curve fitting approach.

In Table 5 and 6, we present results of band fitting for both copolymers at different water activities. There is some controversy in the literature about assigning the band corresponding to free water. Cotugno et al. assigned the resolved peak appeared at the highest frequency (3629 cm^{-1}) to unassociated water in an epoxy resin matrix.[19] Sutandar et al., in analyzing the state of water absorbed in poly(methyl methacrylate) films, assigned the peak that appeared at the lowest frequency (3382 cm^{-1}) to free water in the film.[16]

Table 5 and 6 show that at lower relative humidities, the lower frequency peak (at 3280 cm^{-1} for $P(BA_{50}MMA_{49})$ and at 3336 cm^{-1} for $P(EHA_{50}tBMA_{49})$) disappears. Therefore, we assigned the low frequency peaks to unassociated water that does not contribute to the plasticization process. The results show that at 23 and 54% RH, there is no detectable free water in the sample.

With the notion that at 23 and 54% RH almost all of the absorbed water participates in accelerating diffusion, we reconstruct the Fujita plots in Figure 7. Here we fixed the intercept of the plot to the free volume of the polymer at 25 °C. We present, for comparison, the points corresponding to 85 and 98% RH on the same plot. As illustrated by the shaded envelop, at low values of $(\varphi_w)^{-1}$, phase-separated water is more significant for $P(EHA_{50}tBMA_{49})$. On the basis of this analysis, we calculated the β value to be 0.36 for $P(BA_{50}MMA_{49})$ and 0.19 for $P(EHA_{50}tBMA_{49})$. These values are significantly larger than what has been reported for common plasticizers such as Texanol (with $\beta \sim 0.07$).[54] More importantly, they lay within the theoretical expectation of Fujita−Doolittle model.

Summary and Conclusions

We examined the influence of humidity on the diffusion rate for copolymers of BA/MMA and EHA/tBMA. These copolymers were designed to have similar glass transition temperature but different hydrophilicity. By studying diffusion rate

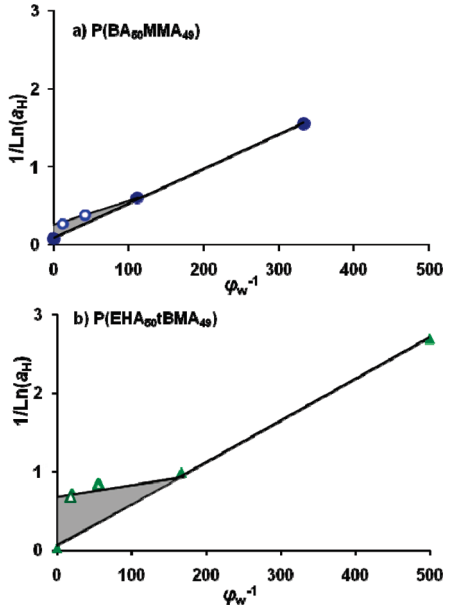

Figure 7. Reconstructed Fujita plots based on the dual nature of water. The dashed area represents the phase-separated water in the films.

at different temperatures, we obtained TTS shift factors that correlate with those obtained from the bulk polymer by rheology measurements. In addition, the shift factors comply with a linear increase of the free volume with temperature and can be fitted with the WLF equation. The WLF constants provided us with the important parameter $1/C_1$ at 25 °C, which corresponds to the fractional free volume of each copolymer at 25 °C.

To analyze the polymer diffusion rates at different relative humidities, we used a master curve analysis based upon humidity-related shift factors. We showed that these raw shift factors do not comply with the assumption of a linear increase in the free volume with the mass (volume) fraction of water absorbed by the sample. On the basis of the observation of turbidity of the films and FTIR measurements, we confirmed the presence of free water in the films at high humidities. This fraction of water does not contribute to plasticization. To compare the efficiency of water in promoting diffusion rate, we analyzed the data in the framework of the Fujita−Doolittle model. Meaningful β parameters were obtained only after the presence of free water in the film was taken into account. The results showed that molecularly dispersed water is much more efficient in promoting diffusion in latex films than other well-known plasticizers.

We envision two mechanisms by which water promotes polymer diffusion rates in these polymer films. First, water contributes to the free volume of the film as a consequence of its low glass transition temperature. Water shows weak glass forming signatures,[56] and thus it is challenging to measure accurately its glass transition temperature. Values between 120 to 160 K have been reported in the literature. The most widely adopted value is 136 K.[57] Thus, water is characterized by a much lower T_g than conventional plasticizers. Hence, even at very low volume fractions, water molecules can contribute significantly to the free volume of the system and cause extensive plasticization at room temperature.

The second mechanism is associated with the presence of −COOH groups in the latex polymer. In the absence of water, the presence of −COOH groups slows down the rate of polymer diffusion,[58] presumably because of hydrogen bonding between the acidic −OH and the ester carbonyl groups of the polymer molecules. One can imagine that in films containing water, the water molecules can compete with the carboxylic acid groups in the latex polymer in forming hydrogen bonds with these ester C=O groups. In this way, water can lubricate the diffusion process. At this point, it is not clear to us which mechanism is dominant. Performing the same experiments with dispersions synthesized without any MAA added may be helpful in this regard.

Acknowledgment. The authors thank Rohm and Haas Co. (now Dow Advanced Materials), Rohm and Haas Canada, and NSERC Canada for their support of this research.

Supporting Information Available: Text including the equations used for Monte Carlo simulations and figures showing plots of the energy transfer efficiency and the fraction of mixing versus time for samples annealed at different temperatures, plots of $\ln(D_{app})$ vs $1/T$ at two different fraction of mixing, rheology master curves for both copolymers, Fujita plots in which the intercept was fixed at the pure polymer free volume, transmission FTIR spectra of copolymer films aged at different relative humidity, and examples of FTIR curve fitting analysis. This material is available free of charge via the Internet at http://pubs.acs.org.

References and Notes

(1) Struik, L. C. E. *Physical Aging in Amorphous Polymers and Other Materials*; Elsevier: Amsterdam, 1978.
(2) Bley, O.; Siepmann, J.; Bodmeier, R. *J. Pharm. Sci.* **2009**, *98*, 651–664.
(3) Chang, R. K.; Raghavan, K. S.; Hussain, M. A. *J. Pharm. Sci.* **1998**, *87*, 556–558.
(4) Kuentz, M.; Röthlisberger, D. *Int. J. Pharm.* **2002**, *236*, 145–152.
(5) Cole, E. T.; Cadé, D.; Benameur, H. *Adv. Drug Delivery Rev.* **2008**, *60*, 747–756.
(6) Kinloch, A. J.; Korenberg, C. F.; Tan, K. T.; Watts, J. F. *J. Mater. Sci.* **2007**, *42*, 6353–6370.
(7) Tan, K. T.; Vogt, B. D.; White, C. C.; Steffens, K. L.; Goldman, J.; Satija, S. K.; Cleric, C.; Hunston, D. L. *Langmuir* **2008**, *24*, 9189–9193.
(8) Jubete, E.; Liauw, M.; Allen, N. *Prog. Org. Coat.* **2007**, *59*, 126–133.
(9) Mijovic, J.; Lin, K. *J. Appl. Polym. Sci.* **1985**, *30*, 2527.
(10) Banks, L.; Ellis, B. *Polym. Bull.* **1979**, *I*, 377.
(11) Brinke, G.; Karasz, F. E.; Ellis, T. S. *Macromolecules* **1983**, *16*, 244–249.
(12) Jelinski, L. W.; Dumais, J. J.; Cholli, A. L.; Ellis, T. S.; Karasz *Macromolecules* **1985**, *18*, 1091–1095.
(13) Ellis, T. S.; Karasz, F. E. *Polymer* **1984**, *25*, 664–669.
(14) Couchmann, P. R.; Karasz, F. E. *Macromolecules* **1978**, *11*, 117–119.
(15) Dias, C. R.; Rosa, M. J.; Pinho, M. N. *J. Membrane Sci.* **1998**, 259–267.
(16) Sutandar, P.; June Ahn, D.; Franses, E. I. *Macromolecules* **1994**, *27*, 7316–7328.
(17) Hodge, R. M. *Polymer* **1996**, *37*, 1371–1376.
(18) Hodge, R. M.; Bastow, T. J.; Edward, G. H.; Simon, G. P.; Hill, A. J. *Macromolecules* **1996**, *29*, 8137–8143.
(19) (a) Musto, P.; Ragosta, G.; Mascia, L. *Chem. Mater.* **2000**, *12*, 1331–1341. (b) Cotugno, S.; Mensitieri, G.; Musto, P.; Sanguigno, L. *Macromolecules* **2005**, *35*, 801–811.
(20) Zhou, J.; Lucas, J. *Polymer* **1999**, 5505–5512.
(21) Wang, B.; Gong, W.; Liu, W. H.; Wang, Z. F.; Qi, N.; Li, X. W.; Liu, M. J.; Li, S. J. *Polymer* **2003**, *44*, 4047–4052.
(22) Soles, C.; Chang, F. T.; Gidley, D. W.; Yee, A. F. *J. Polym. Sci., Part B: Polym. Phys.* **2000**, *38*, 776–791.
(23) (a) Mijovic, J.; Zhang, H. *Macromolecules* **2003**, *36*, 1279. (b) Zhang, H.; Mijovic, J. *Macromolecules* **2004**, *37*, 5844–5846.
(24) Sperry, P. R.; Snyder, B. S.; O'Dowd, M. L.; Lesko, P. M. *Langmuir* **1994**, *10*, 2619–2628.
(25) Lin, F.; Meier, D. J. *Langmuir* **1996**, *12*, 2774–2780.
(26) Lin, F.; Meier, D. J. *Langmuir* **1995**, *11*, 2726–2733.
(27) Rottstegge, J.; Traub, B.; Wilhelm, M.; Landfester, K.; Heldmann, C.; Spiess, W. *Macromol. Chem. Phys.* **2003**, *204*, 787–802.
(28) Veniaminov, A.; Eckert, T.; Sillescu, H.; Bartsch, E. *Macromolecules* **2003**, *36*, 4944–4953.

(29) Veniaminov, A.; Jahr, T.; Sillescu, H.; Bartsch, E. *Macromolecules* **2002**, *35*, 808–819.
(30) Nawaz, Q.; Rharbi, Y. *Macromolecules* **2008**, *41*, 5928–5933.
(31) Turshatov, A.; Adams, J.; Johannsmann, D. *Macromolecules* **2008**, *41*, 5365–5372.
(32) Sosnowski, S.; Feng, J.; Winnik, M. A. *J. Polym. Sci., Part A: Polym. Chem.* **1994**, *32*, 1497–1505.
(33) Tronc, H.; Liu, R.; Winnik, M. A.; Eckersley, S. T.; Rose, G. D.; Weichuhn, J. M.; Meunier, D. M. *J. Polym. Sci., Part A: Polym. Chem.* **2002**, *40*, 2609–2625.
(34) Pathak, J. A.; Colby, R. H.; Kamath, A. Y.; Kumar, S. K.; Stadler, R. *Macromolecules* **1998**, *31*, 8988.
(35) Koenig, J. L. *Spectroscopy of Polymers*; American Chemical Society: Washington, DC, 1992.
(36) James, D. R.; Demmer, D. R. M.; Verrall, R. E.; Steer, R. P. *Rev. Sci. Instrum.* **1983**, *54*, 1121–1130.
(37) Greenspan, L. *J. Res. NBS A Phys. Chem.* **1977**, *81A*, 89.
(38) Oh, J. K.; Wu, J.; Winnik, M. A.; Craun, G. P.; Rademacher, J.; Farwaha, R. *J. Polym. Sci., Part A: Polym. Chem.* **2002**, *40*, 3001–3011.
(39) O'Connor, D. V.; Phillips, D. *Time-Correlated Single Photon Counting*; Academic Press: New York, 1984.
(40) Liu, Y.; Haley, J. C.; Deng, K.; Lau, W.; Winnik, M. A. *Macromolecules* **2007**, *40*, 6422–6431.
(41) Bartels, C. R.; Buckley, C.; Graessley, W. W. *Macromolecules* **1984**, *17*, 2702–2708.
(42) Crank, J. *The Mathematics of Diffusion*; Clarendon: Oxford, England, 1975.
(43) Yang, J.; Winnik, M. A. *J. Phys. Chem. B* **2005**, *109*, 18408–18417.
(44) Haley, C. J.; Liu, Y.; Winnik, M. A.; Demmer, D.; Haslett, T.; Lau, W. *Rev. Sci. Instrum.* **2007**, *78*, 084101.
(45) Wu, J.; Tomba, J. P.; Winnik, M. A.; Farwaha, R.; Radmacher, J. *Macromolecules* **2004**, *37*, 2299.
(46) Oh, J. K.; Yang, J.; Tomba, J. P.; Winnik, M. A.; Farwaha, R.; Radmacher, J. *Macromoleculs* **2003**, *36*, 8836.
(47) Farinha, J. P. S.; Vorobyova, O.; Winnik, M. A. *Macromoleculs* **2000**, *33*, 5863–5873.
(48) Ferry, J. D. *Viscoelastic Properties of Polymers*; Wiley: New York, 1980.
(49) Haley, J. C.; Liu, Y.; Winnik, M. A.; Lau, W. *J. Coat. Technol. Res.* **2008**, *5*, 157–168.
(50) (a) Yildiz, M. E.; Kokini, J. L. *J. Rheol.* **2001**, *45*, 903–912. (b) Ogawa, T.; Inoue, A.; Osawa, S. *J. Appl. Polym. Sci.* **1998**, *69*, 315–321.
(51) Hancock, B.; Zografi, G. *Pharm. Res.* **1994**, *11*, 471–477.
(52) Fujita, H. *Fortschr. Hochpolym.-Forsch.* **1961**, *3*, 1.
(53) Odrobina, E.; Feng, J.; Winnik, M. A. *J. Polym. Sci., Part A: Polymer Chemistry* **2000**, *38*, 3933.
(54) Juhué, D.; Wang, Y.; Winnik, M. A. *Makromol. Chem. Rapid Commun.* **1995**, *16*, 861.
(55) Maddams, W. F. *Appl. Spectrosc.* **1980**, *34*, 245.
(56) Angell, C. A. *Science* **2008**, *319*, 582–587.
(57) Johari, G. P. *J. Chem. Phys.* **2003**, *119*, 2935–2937.
(58) Kim, H.-B.; Wang, Y.; Winnik, M. A. *Polymer* **1994**, *35*, 1779–1786.